Structural characteristics and gel properties of pectin from citrus physiological premature fruit drop

Tingting Qi [a], Jingnan Ren [a], Xiao Li [a], Qi An [a], Nawei Zhang [a], Xiao Jia [a], Siyi Pan [a], Gang Fan [a,*], Zhifeng Zhang [b], Kangning Wu [b]

[a] *Key Laboratory of Environment Correlative Dietology, Ministry of Education; Hubei Province Key Laboratory of Fruit & Vegetable Processing & Quality Control, College of Food Science and Technology, Huazhong Agricultural University, Wuhan 430070, China*
[b] *Ningxia Huaxinda Health Technology Co., Ltd., Lingwu 751400, China*

ARTICLE INFO

ABSTRACT

This study is the first to extract and characterize pectin from citrus physiological premature fruit drop. The extraction yield of pectin reached 4.4 % by acid hydrolysis method. The degree of methoxy-esterification (DM) of citrus physiological premature fruit drop pectin (CPDP) was 15.27 %, indicating it was low-methoxylated pectin (LMP). The monosaccharide composition and molar mass test results showed CPDP was a highly branched macromolecular polysaccharide (β: 0.02, Mw: 2.006×10^5 g/mol) with rich rhamnogalacturonan I domain (50.40 %) and long arabinose and galactose side chain (32.02 %). Based on the fact that CPDP is LMP, Ca^{2+} was used to induce CPDP to form gels. Textural and rheological tests showed that the gel strength and storage modulus of CPDP were higher than commercial citrus pectin (CP) used in this paper due to the lower DM and rich neutral sugar side chains of CPDP. Scanning electron microscope (SEM) results showed CPDP had stable gel network structure.

1. Introduction

Citrus is a Genus in the Rutaceae family. It is a common phenomenon that a lot of citrus premature fruits drop off from the tree during growth which is so-called citrus physiological premature fruit drop. The fruit setting rate of citrus is low, generally 3–5 %. The high-yield trees can reach about 10 %, and low-yield trees are usually <1 %. However, citrus physiological premature fruit drop is usually discarded directly without being utilized, which not only causes waste of resources, but also causes environmental pollution. So if the citrus physiological premature fruit drop can be used as raw material to extract pectin, the waste resources can be effectively utilized and the added value can be increased. Pectin is a multifunctional food ingredient widely used in food industry, pharmaceutical industry, and in packaging regimes (Zhao, Kim, & Cameron, 2022). Pectin is commonly used in the food industry as an additive in foods such as gelling agents, thickeners, emulsifiers, jellies, jams, and low-calorie foods. Pectin is widely used in the pharmaceutical industry for immune regulation, intestinal flora regulation, anti-inflammatory, atherosclerosis prevention, anti-diabetes, anti-obesity, antitussive, analgesic, wound healing, and cancer treatment. Pectin is

also used in many other industries, such as the preparation of edible films and paper substitutes (Chandel et al., 2022; Zhang et al., 2021).

Pectin is a kind of acidic heteropolysaccharide widely existing in plant cell wall (Thakur, Singh, & Handa, 1997). It mainly includes three types of structures: homogalacturonan (HG, smooth region), Rhamnogalacturonan I (RG-I, hairy region), and rhamnogalacturonan II (RG-II) (O'Neill, Albersheim, & Darvill, 1990; Santos et al., 2020). HG is composed of α-(1,4)-D- galacturonic acid, which constitutes the linear backbone of pectin. RG-I is the main branching structure of the pectin molecule and is composed of a repeating dimer of rhamnose (Rha) and galacturonic acid (GalA), of which the Rha has branched chains of varying lengths composed of Ara and Gal (Makshakova, Safarova, & Zuev, 2021). RG-II is a secondary branching structure of pectin containing at least seven α-D-GalA residues in the HG backbone, which can be replaced by four complex oligosaccharides side chains (Colodel, Vriesmann, & Lucia, 2019; Ridley, O'Neill, & Mohnen, 2001). The degree of methyl-esterification (DM) is the ratio of methyl esterified carboxylic acid to total carboxylic acid. Pectins can be classified into high-methoxylated pectins (HMP, DM > 50 %) and LMP (DM < 50 %) according to DM (Thakur et al., 1997). DM is the main factor that

---

* Corresponding author.
E-mail address: fangang@mail.hzau.edu.cn (G. Fan).

determines the functionality of pectin, especially gel properties. In general, HMP gels are obtained at acidic pH (typically lower than 3.5) in the presence of a high sucrose concentration or other co-solutes (Dasilva, Goncalves, & Rao, 1995). Therefore, HMP is usually used for a thickening agent in the production of foods with high sugar content. In contrast, LMP can be induced by divalent cations (Ca^{2+}, Fe^{2+}, etc.) in a wide range of pH and can form gels without sugar (Wan et al., 2021). So LMP can be used in the production of low-sugar and low-calorie foods and has a broad market prospect.

Pectin in nature is generally HMP, and natural LMP is rare. Natural LMP is mainly derived from sunflower discs (Kang, Hua, Yang, Chen, & Yang, 2015). The LMP currently on the market is mainly obtained indirectly through HMP de-esterification (Wan et al., 2019). Therefore, it is of great importance to find new raw materials rich in LMP. This study aims to verify whether CPDP is LMP or HMP, it would be an interesting discovery if the CPDP is LMP.

There are various extraction methods for pectin, mainly including acid extraction (Cho et al., 2019), alkali extraction and biological enzyme method (Cui et al., 2020), steam blasting method (Zhao, Wang, Zeng, & Xu, 2021), ultrasonic assisted method (Hosseini, Khodaiyan, Kazemi, & Najari, 2019), microwave assisted method (Su et al., 2019), and a new technology for extracting citrus pectin based on the interaction between sodium caseinate and pectin (Ren et al., 2019). Acid hydrolysis is the most widely used method for pectin extraction, which has the advantages of easy operation, low cost and environmental protection. It is suitable for large-scale industrial production.

There are no reports on pectin extraction from citrus physiological premature fruit drop. Therefore, this study was conducted to extract and characterize pectin from citrus physiological premature fruit drop. The structure of pectin was characterized (monosaccharide composition, molecular weight, fourier transform infrared (FTIR), spectroscopy and nuclear magnetic resonance (NMR), spectroscopy) and the DM, particle size and zeta potential, rheological properties and gel properties (gel strength, rheology and microstructure) of pectin were determined. This will improve the utilization of waste fruits and expand the sources of pectin.

2. Materials and methods

2.1. Materials

Citrus physiological premature fruit drop (*Citrus sinensis* (L.) Osbeck) with a diameter of about 0.5–1.3 cm was provided by Zigui County Qugu Food Co. Ltd. (Zigui, China). Commercial citrus pectin (CP, P9135, GalA ≥74.0 %) was purchased from Sigma-Aldrich (St. Louis, USA). L-fucose (Fuc), L-rhamnose (Rha), L-arabinose (Ara), D-galactose (Gal), D-xylose (Xyl), D-mannose (Man), D-fructose (Fru), galacturonic acid (GalA), D-glucuronic acid (GlcA) and other standard products were purchased from Yuanye Biotechnology Co., Ltd. (Shanghai, China). All the other reagents used were of analytical grade.

2.2. Extraction and purification of pectin

The extraction of pectin was referred to Zhang et al. (2021) with some modifications. The whole naturally air-dried citrus physiological premature fruit drop was crushed with a high-speed multifunctional grinder (Yunbang, YB-300, China) and passed the 60 meshes sieve to obtain 250 μm powder for standby. The powder was mixed with 15 times the volume of distilled water, and the pH of the mixed solution was adjusted to 1.5 with 1 mol/L HCl. Then the mixture was placed in a constant temperature water bath at 100 °C for 120 min with constant stirring at 250 rpm , and then centrifuged at 5000 *g* for 10 min at 20 °C using a high speed refrigerated centrifuge (Beckman, Avanti JXN-26, USA) to obtain the supernatant. An equal volume of 95 % ethanol was added to the supernatant and left for 1 h. The precipitated pectin was obtained by centrifugation at 5000 *g* for 10 min at 20 °C and washed

twice with 95 % ethanol. Finally, the pectin was obtained by freeze-drying.

$$\text{Pectin extraction yield (\%)} = \frac{M_1}{M_2} \times 100 \qquad (1)$$

M_1 is the dry weight of extracted pectin (g); M_2 is the dry weight of citrus physiological premature fruit drop powder (g).

2.3. DM determination

The DM of pectin was determined using the NaOH titration method based on the method described by Jafari, Khodaiyan, Kiani, and Hosseini (2017) and verified by the area of the absorption peaks of pectin at 1630 cm^{-1} (Aera$_{1630}$) and 1748 cm^{-1} (Aera$_{1748}$) in the FTIR spectrum (Pan et al., 2022).

For this purpose, 0.1 g of pectin was moistened with 2 mL of anhydrous ethanol and dissolved in 100 mL carbon dioxide-free water which was obtained by boiling distilled water for 10 min. Then three drops of phenolphthalein reagent were added and the sample was titrated with 0.1 mol/L NaOH. The volume of NaOH used to the titration end point was recorded as V_1. Subsequently, 20 mL of 0.5 mol/L NaOH was added to the solution, and the solution was shaken vigorously with a plug for 15 min. Then 20 mL of 0.5 mol/L HCl solution was added for the completely neutralization of the 0.5 mol/L NaOH and the solution was shaken vigorously. Three drops of phenolphthalein reagent were added again and the solution was titrated with 0.1 mol/L NaOH until the solution became light red. The volume of NaOH consumed was recorded as V_2.

The formulas for calculating the DM of pectin are:

$$DM = \frac{V_2}{V_1 + V_2} \times 100\% \qquad (2)$$

$$DM = \frac{Aera_{1748}}{Area_{1748} + Area_{1630}} \times 100\% \qquad (3)$$

2.4. Structural characteristics of pectin

2.4.1. Determination of monosaccharide composition

The monosaccharide composition of the pectin was analyzed by high-performance anion-exchange chromatography (HPAEC) (ICS5000, Thermo Fisher Scientific, USA) on a CarboPac PA-20 anion-exchange column (3 × 150 mm, Dionex) using a pulsed amperometric detector (PAD, Dionex ICS 5000 system) according to the method described by Guo, Guo, Yu, and Kong (2018), with slight modifications. The injection volume, flow rate and column temperature were set to 5 μL, 0.5 mL/min and 30 °C, respectively. Mobile phases A, B and C were H_2O, 0.1 mol/L NaOH and 0.1 mol/L NaOH with 0.2 mol/L NaAc, respectively. Gradient program was 95:5:0 at 0 min, 85:5:10 at 26 min, 85:5:10 at 42 min, 60:0:40 at 42.1 min, 60:40:0 at 52 min, 95:5:0 at 52.1 min and 95:5:0 at 60 min.

Firstly, 10 mg/mL single standard mother liquor (Fuc, Rha, Ara, Gal, Glc, Xyl, Man, Fru, GalA and GlcA) was prepared and diluted to different concentrations (0.4, 0.8, 4, 8, 16, 24, 32 and 40 μg/mL) of the mixed standard, as shown in Table 1. The experiments were conducted at each concentration to select the appropriate monosaccharide concentration. Then 5 mg pectin sample was hydrolyzed with 1 mL 2 mol/L trifluoroacetic acid solution (TFA) at 121 °C for 2 h and dried with nitrogen. The residue was re-dissolved with ultrapure water, filtered through a membrane with a pore size of 0.22 μm, and then tested on the HPAEC. The monosaccharide composition was determined according to the retention time of chromatographic peaks and the content of each monosaccharide was calculated through the standard curve. The content of each monosaccharide is expressed as mol% of the total monosaccharide content.

Table 1
Monosaccharide mixed standard gradient concentration.

Monosaccharide	Concentration (μg/mL)							
Fuc	0.4	0.8	4	8	16	24	32	40
Rha	0.4	0.8	4	8	16	24	32	40
Ara	0.4	0.8	4	8	16	24	32	40
Gal	0.4	0.8	4	8	16	24	32	40
Glc	0.4	0.8	4	8	16	24	32	40
Xyl	0.4	0.8	4	8	16	24	32	40
Man	0.4	0.8	4	8	16	24	32	40
Fru	0.4	0.8	4	8	16	24	32	40
GalA	0.4	0.8	4	8	16	24	32	40
GlcA	0.4	0.8	4	8	16	24	32	40

2.4.2. Molar mass and molecular conformation measurement with SEC-MALLS-RI system

The molar mass and chain conformation parameters of pectin were measured by size exclusion chromatography - multi angle laser light scattering - refractive index system (SEC-MALLS-RI). The SEC columns (Shodex, Tokyo, Japan) is composed of ohpak SB-805 HQ (300 × 8 mm) , ohpak SB-804 HQ (300 × 8 mm) and ohpak SB-803 HQ (300 × 8 mm) in series. The MALLS is DAWN HELEOS II (Wyatt technology, CA, USA). The RI detector is Optilab T-Rex (Wyatt technology, CA, USA). The sample was dissolved in 0.1 mol/L NaNO$_3$ aqueous solution containing 0.02 % NaN$_3$ (w/w) at a final concentration of 1 mg/mL, and filtered through a filter with a pore size of 0.45 μm and then detected on the machine. The mobile phase was 0.1 mol/L NaNO$_3$ solution containing 0.02 % NaN$_3$ and the injection volume was 100 μL. The refractive index (dn/dc), column temperature and flow rate were set to 0.145 mL/g, 45 °C and 0.4 mL/min. The data obtained by SEC-MALLS-RI were analyzed by ASTRA 6.1 software (Wyatt Technology, CA, USA).

The basic light-scattering equation are as follows (Soares et al., 2019):

$$\frac{K \bullet c}{R_\theta} = \frac{1}{M_w} \left(1 + \frac{q^2 <R_G^2>}{3} \right) + 2A2 \cdot c \tag{4}$$

$$K = 4\pi^2 \left(\frac{dn}{dc}\right)^2 \frac{n_0^2}{N_A \lambda_0^4} \tag{5}$$

In Eqs. (4)–(5), K is the optical constant; c is the mass concentration; R_θ is the Rayleigh ratio ; $<R_G^2>$ is the root mean square average radius of gyration; A_2 is the second viral coefficient ; dn/dc is the refractive index increment, n_0 is the refractive index of the solvent; N_A is the Avogadro's number; λ_0 is the wavelength of laser in vacuum.

2.4.3. FTIR spectrometry determination

The dry pectin powder was ground with KBr powder and pressed into thin slices of about 1 mm thickness, and it was tested using FTIR spectrometer (Jasco Inc., Easton, MO) with air as background. The FTIR spectra was obtained over a 4000–400 cm^{-1} wave-number range with 32 scans and a 4 s^{-1} resolution (Zheng et al., 2020).

2.4.4. NMR spectroscopy determination

Samples were deuterium-exchanged by freeze-drying two times and then approximately 10 mg pectin sample was dissolved in 0.55 mL D$_2$O (99.96 %) for analysis by ^{1}H NMR, which was performed at 25 °C through a 600 MHz NMR spectrometer (Bruker, Rheinstetten, Germany). Tetramethylsilane (TMS) was used as internal references (Yan et al., 2021).

2.5. Particle size determination

The particle size (hydrodynamic average diameter, d$_h$) and polydispersity index (PDI) of pectin solutions (1 g/L) were measured with a Zetasizer Nano-ZS90 (Malvern Instruments Ltd., Worcestershire, UK) at 25 °C.

Hydrodynamic diameter distributions were obtained by means of the amplitude of the decay rate A(Γ), which is estimated by fitting the normalized temporal intensity correlation functions, g$^{(2)}$(t), through a NNLS (Non-Negative Least Square) algorithm, according to Eq. (6). Thus, Γ distribution is turned to size by Eqs. (7) and (8) (Ferreira et al., 2022):

$$g^{(2)}(t) = 1 + \beta \left[\int_0^\infty A(\Gamma) \, e^{-\Gamma t} d\Gamma \right]^2 \tag{6}$$

$$\Gamma = \left(\frac{4\pi n_i}{\lambda} sin\frac{\theta}{2}\right)^2 \cdot D \tag{7}$$

$$d_h = \frac{k_B T}{3\pi\eta D} \tag{8}$$

In Eqs. (6)–(8), A and β are constants that depends on the number of coherence areas in the detector, Γ is the decay rate, n_i is the index of refraction of the dispersion, λ is the wavelength of the laser, θ is the angle of detection (173°), D ($nm^2 \bullet s^{-1}$) is the mass diffusivity of the dispersed particles, k_B (1.3806 × 10^{-23} $m^2 \bullet kg \bullet s^{-2} \bullet K^{-1}$) is the Boltzmann constant, T is the temperature and η ($Pa \bullet s$) is the viscosity of the medium, and d_h (nm) is the average hydrodynamic diameter of dispersed particles.

PDI was calculated for each size distribution estimated according to Eq. (9):

$$PDI = \left(\frac{SD}{d_h}\right)^2 \tag{9}$$

In Eq. (9), SD is the standard deviation corresponding to each d_h value.

2.6. Zeta potential determination

The zeta potential (ζ potential) of pectin solutions were measured with a Zetasizer Nano-ZS90. The measurements were conducted in pectin solution (1 g/L) at 25 °C, with the pH in the range of 3.0–7.0 (0.5 mol/L sodium citrate was used for the pH adjustment).

ζ potential was estimated from the electrophoretic mobility of dispersed pectin chains due to a controlled electric field, applied to the systems. Then, the speed and the direction of the particle movement due to this electric field allowed calculating the electrophoretic mobility (Eq. (10)). Finally, the Smoluchowski model for the double electrical layer was considered to calculate the ζ potential values (Eq. (11)) (Galván et al., 2018):

$$\mu_e = \frac{v}{\left|\overrightarrow{E}\right|} \tag{10}$$

$$\zeta = \frac{\eta\mu_e}{\varepsilon_o \varepsilon_r} \tag{11}$$

In Eqs. (8) and (9), μ_e ($m^2 \bullet s^{-1} \bullet V^{-1}$) is the electrophoretic mobility, v ($m \bullet s^{-1}$) is the speed of particles, and $\overrightarrow{E}$ ($mV \bullet m^{-1}$) is the electric field; ε_r (dimensionless) is the dielectric constant of the medium, ε_o ($C^2 \bullet N^{-1} \bullet m^{-2}$) is the permittivity of free space, ζ (mV) is the zeta potential, and η ($Pa \bullet s$) is the viscosity.

2.7. Rheological properties determination of pectin solutions

The rheological properties of pectin solutions were measured using a rotational rheometer (AR2000ex, TA Instruments, USA) according to the method of a previous study (Nguyen, Nguyen, & Savage, 2019). Pectin solutions (20 g/L and 30 g/L) were prepared and placed in a cone and plate geometry (40 mm diameter, 2°). The apparent viscosity of pectin solutions was measured at 25 °C with a shear rate from 0.1 to 100 s^{-1}.

2.8. Gel properties determination

2.8.1. Preparation of pectin gels

The preparation of pectin gels was performed according to the method of Munoz-Almagro, Villamiel, Wilde, Gunning, & Montilla, 2021 with slight modification. The pectin gels were formed in cylindrical glass vials (25 mm diameter, 50 mm height). Pectin (20 g/L) and sucrose (30 %, *w/v*) were dissolved in distilled water, heated and stirred (50 °C, 200 rpm/min) in a thermostatically heated magnetic stirrer (Changcheng, DF-101S, China) until completely dissolved. The pH of the pectin solution was adjusted to 4.0 with citric acid or trisodium citrate dihydrate (0.5 mol/L). Then, $CaCl_2$ solution (0.5 mol/L) was added to the pectin solution preheated to 80 °C to bring the Ca^{2+} concentration to 30 mg/g and quickly stirred evenly, and stored at 4 °C for 24 h to form a stable gel.

Based on the above method, pectin gel was prepared by adjusting pectin concentration to 5–25 g/L, Ca^{2+} concentration to 10–50 mg/g, pH value to 2.0–7.0 and sucrose concentration to 10–50 %.

2.8.2. Determination of gel strength

The gel strength of pectin was measured using a TA-XT Plus Texture Analyzer (Stable Micro Systems, Robbinsville, NJ, USA) according to the method of Zhang et al., 2022 with some modifications. A cylindrical probe (P 0.5 type, 15 mm diameter) was used to penetrate the gel (cylinder with a diameter of 25 mm and a height of 20 mm) to a depth of 4 mm from the gel surface with a trigger force of 5 g and a constant speed of 1 mm/s. Gel strength is the stress value on the probe at the 4 mm depth (Han et al., 2017).

2.8.3. Determination of dynamic rheological properties

A temperature sweep was performed to investigate the effect of temperature on the rheological behavior of pectin gels using a rotational rheometer with a cone plate geometry (2°, 40 mm diameter) according to the method of Huang et al., 2020 with some modifications. This study was carried out under the conditions of pectin concentration of 20 g/L, pH = 4 and Ca^{2+} concentration of 30 mg/g. The pectin solution was heated to 95 °C before adding $CaCl_2$ solution to avoid the formation of pre-gel, and then the well-mixed solution was added to the plate preheated to 95 °C. Temperature sweep was performed at a strain of 5 % (in the linear viscoelastic region) and a frequency of 1 Hz at a rate of 5 °C/min to record the change of the storage modulus (G') and loss modulus (G'') from 95 °C to 5 °C. The linear viscoelasticity range was determined by amplitude sweep test from 0.01 % to 100 % at a constant frequency of 1 Hz (Cai, Hu, & Huang, 2021).

The thermally reversible properties of pectin gels were studied by heating from 5 °C to 95 °C. The changes of G' and G'' of the pectin gels during this period were recorded. Throughout the experiment, a thermal insulation cover was placed on the cone plate, and silicone oil was applied to the gap and the edge of the thermal insulation cover to prevent moisture loss (Cheng, Wang, Zhang, Zhai, & Hou, 2021).

Frequency sweep was conducted from 0.1 to 10 Hz at 5 °C with a strain of 1 % (in the linear viscoelastic region) to measure the variation of both moduli with the frequency. The linear viscoelasticity range was determined by amplitude sweep test from 0.01 % to 100 % at a constant frequency of 10 Hz.

2.8.4. Field-emission scanning electron microscope (FE-SEM)

The morphology of the pectin gels was observed by FE-SEM (SU8010, Jeol, Japan) according to the method of Qiu, Huang, Li, Ma, & Wang, 2018 with slight modifications. The prepared pectin gels were pre-frozen at −80 °C for 24 h to avoid collapse of the gel structure and then freeze-dried. The dried samples were cut into 3 mm squares of approximately 1 mm thickness and glued to a conductive adhesive on a steel table. Then, the samples were coated with a thin conductive gold for observation.

2.9. Statistical analysis

All experiments were conducted three times and the data were reported as the means values ± standard deviation (SD). The statistical differences between data were analyzed by Analysis of variance (ANOVA) and Tukey's test at a 5 % significance level by SPSS 21 (IBM, New York, USA). The figures were plotted via Origin 9.0 (OriginLab Inc., Northampton, Massachusetts, USA).

3. Results and discussion

3.1. DM of CPDP

As shown in Table 2, the DM of CPDP was <50 % (15.27 % by the titrimetric method and 14.67 % by the FTIR), indicating that CPDP belongs to LMP, which is an interesting finding. This is different from pectin extracted from citrus peel residue by traditional acid method. Previous studies have shown that the pectin extracted from citrus peel residue is HMP (Wang, Chen, & Lu, 2014). The gel mechanism of pectin is closely related to its DM value. HMP requires a large amount of sugar to form a gel under acidic conditions. Whereas LMP can form gel when mediated by Ca^{2+} without sugar (Fraeye, Duvetter, Doungla, Van Loey, & Hendrickx, 2010). Therefore, CPDP has great application potential in the low-calorie healthy food market.

3.2. Structural characterization

3.2.1. Monosaccharide composition analysis

The monosaccharide composition of CPDP and CP is shown in Fig. 1. GalA was the predominant component in CPDP and CP, accounting for 50.56 % and 68.74 % respectively (Table 3), respectively. It can be seen that CPDP had a higher content of neutral sugars, especially Ara and Gal, accounting for 9.31 % and 22.71 %, respectively, which was much higher than the content of Ara (2.54 %) and Gal (13.50 %) in CP. The molar ratio of Rha/GalA indicated the contribution of RG-I to pectin population. The (Ara + Gal)/Rha reflected the average length of RG-I side chains (Li et al., 2019; Wang et al., 2016). The molar ratio of Rha/GalA in CPDP (0.18) was higher than that of CP (0.13), indicating that CPDP has more abundant RG-I region. The (Ara + Gal)/Rha ratio of CPDP was high (3.48), almost twice that of CP (1.85), indicating that CPDP has longer RG-I side chains than CP. The molar ratio of RG-I in CPDP was as high as 50.4 %, indicating the presence of abundant "hairy areas" in its structure. These results suggested that the CPDP has abundant RG-I structural domains with long Ara and Gal side chains.

#### 3.2.2. Molar mass and chain conformation analysis

The molar mass distribution chromatograms of CP and CPDP are shown in Fig. 2A and B. The LS signal is used in conjunction with the RI signal to determine molar mass and radius of gyration. The molar mass distribution of CPDP had a wider range (1.0×10^4 - 1.0×10^7 g/mol) than CP (5.0×10^4 - 2.0×10^6 g/mol). The Mw and PDI of CPDP were higher than that of CP, which was attributed to the fact that CPDP contained more rhamnose (Nakauma et al., 2008). The values in Table 4 show more accurate information about the molecular size of pectin. Rw, Rn, and Rz refer to weight-, number-, z-average mean square radius of gyration, respectively. The radius Rw (32.7 nm) and Rn (34.6 nm) of CPDP were higher than Rw (25.1 nm) and Rn (17.9 nm) of CP, respectively. This is the same result as that revealed in the previous study: the molecular weight of pectin increases with the increase of molecular radius (Chen et al., 2016). The Rz of CPDP was slightly lower than that of CP, which may be due to the different monosaccharide composition and molecular structure of the two pectins. Previous studies have indicated that pectin containing higher Ara had larger molar mass but smaller Rz than those containing higher GalA (Nakauma et al., 2008).

The molecular conformations of the two pectins in aqueous solution are shown in Fig. 2C and D. The chain conformation of the pectin in

Table 2

Degree of methylation, particle size, polydispersity index (PDI) and zeta potential of CP and CPDP. Data are presented as "mean ± standard deviation", n = 3. Different capital letters in the same column and different lowercase letters in the same row indicate a significant difference (p < 0.05).

Pectin	Degree of methylation (%)		Size (nm)	PDI	Zeta potential (mV)				
	Titration	FTIR			pH 3	pH 4	pH 5	pH 6	pH 7
CP	39.12 ± 0.85[aA]	38.07 ± 1.65[aA]	1243 ± 10[B]	0.20 ± 0.05[A]	−11.47 ± 0.40[dA]	−26.63 ± 0.39[cA]	−35.20 ± 0.29[aA]	−35.03 ± 0.58[aA]	−30.13 ± 1.56[bA]
CPDP	15.27 ± 0.42[aB]	14.67 ± 0.56[aB]	2099 ± 35[A]	0.32 ± 0.14[A]	−12.20 ± 0.50[cA]	−20.43 ± 0.82[bB]	−29.53 ± 0.34[aB]	−33.57 ± 0.98[aA]	−33.53 ± 3.79[aA]
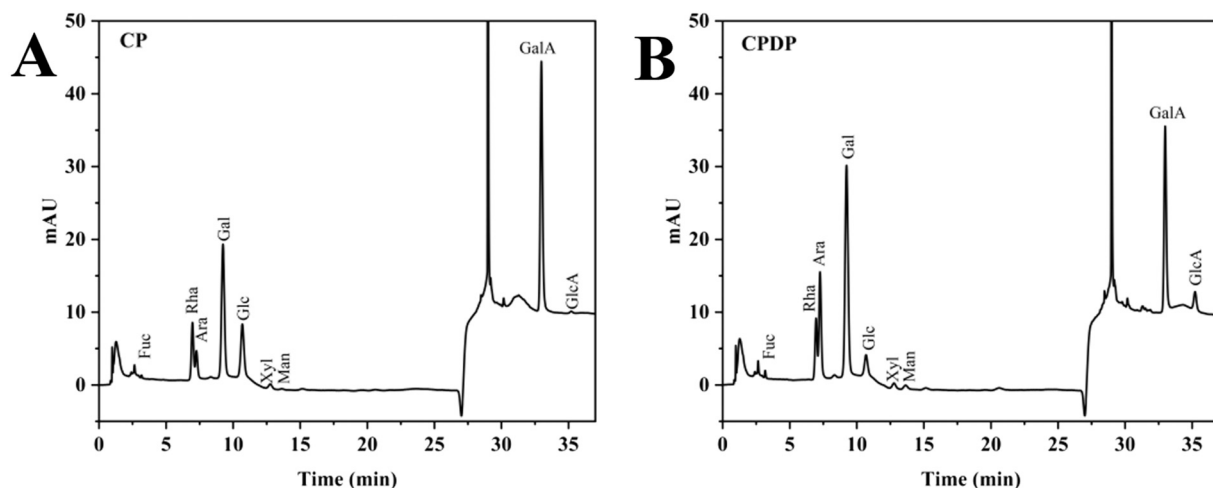
Fig. 1. Monosaccharide composition of CP (A) and CPDP (B).

Table 3

Monosaccharide composition of CP and CPDP.

Monosaccharide composition	CPDP	CP
Fuc (mol %)	0.38 ± 0.01[a]	0.14 ± 0.02[b]
Rha (mol %)	9.19 ± 0.04[a]	8.65 ± 0.34[a]
Ara (mol %)	9.31 ± 0.02[a]	2.54 ± 0.17[b]
Gal (mol %)	22.71 ± 0.02[a]	13.50 ± 0.34[b]
Glc (mol %)	2.46 ± 0.02[b]	5.45 ± 0.17[a]
Xyl (mol %)	0.51 ± 0.01[a]	0.42 ± 0.01[a]
Man (mol %)	0.58 ± 0.02[a]	0.12 ± 0.00[b]
GalA (mol %)	50.56 ± 0.11[b]	68.74 ± 0.18[a]
GlcA (mol %)	4.30 ± 0.00[a]	0.44 ± 0.01[b]
HG (%)[1]	41.37 ± 0.15[b]	60.09 ± 0.16[a]
RG-I (%)[2]	50.40 ± 0.12[a]	33.34 ± 0.85[b]
Rha/GalA[3]	0.18 ± 0.00[a]	0.13 ± 0.00[b]
(Ara + Gal)/Rha[4]	3.48 ± 0.01[a]	1.85 ± 0.05[b]

Fuc: fructose; Rha: rhamnose; Ara: arabinose; Gal: galactose; Glc: glucose; Xyl: xylose; Man: mannose; GalA: galacturonic acid; GlcA: glucuronic acid; HG: homogalacturonan; RG-I: rhamnogalacturonan I.

Data are presented as "mean ± standard deviation", n = 3. Different lowercase letters in the same row indicate a significant difference between the CPDP and CP (p < 0.05).

[1] GalA% – Rha%.
[2] 2Rha% + Ara% + Gal%.
[3] The contribution of RG-I to pectin population.
[4] Average length of RG-I side chains.

aqueous solution was related to the slope (β) between molar mass and root mean square radius of gyration (RMS) (Wyatt, 1993). When the exponent β ≤ 0.33, the pectin in aqueous solution has a tight and uniform spherical conformation, which is a branched pectin. When the exponent β is 0.5–0.6, the pectin in aqueous solution shows a random coil conformation, which is a linear pectin. When the exponent β is 1, the pectin in aqueous solution shows a rigid rod conformation (Wu et al., 2014; Xu, Xu, Xu, & Zhang, 2012). The exponent β of the CP was 0.29,

indicating that it shows a tight and uniform spherical conformation in aqueous solution, belonging to a branched polymer. The exponent β of the CPDP was only 0.02, which is much lower than that of CP, indicating that CPDP exhibits a more compact spherical conformation than CP in aqueous solution, and the RMS-Molar mass relationship plot of CPDP shows a "U-shaped" curve, further indicating that it is a highly branched polymer (Zhao, Chai, Li, Chen, & Tang, 2014). This is consistent with the results of the monosaccharide composition test.

3.2.3. Fourier transform infrared (FTIR) spectroscopy analysis

The FTIR spectroscopy of CPDP and CP of citrus are shown in Fig. 3A. The broad peak at 3470 cm^{-1} came from the stretching vibration of intramolecular and intermolecular O—H, and the absorption peak near 2940 cm^{-1} was the stretching vibration of C—H (mainly including CH, CH$_2$ and CH$_3$) (Deng et al., 2020). The peak at 1748 cm^{-1} was the esterified carboxyl functional group absorption peak (—COOR) and the peak at 1630 cm^{-1} was the free carboxyl functional group absorption peak (—COOH) (Santos et al., 2020). The characteristic peaks of pectin at 1748 cm^{-1} and 1630 cm^{-1} can also be used to distinguish whether the pectin is HMP or LMP (Szymanska-Chargot, Chylinska, Kruk, & Zdunek, 2015). The pectin obtained in this experiment was weakly absorbed at 1748 cm^{-1} and strongly absorbed at 1630 cm^{-1}, so the CPDP is LMP, which is also proved by the methoxylated determination of pectin by titration. The absorption peak of 1440 cm^{-1} was the bending vibration of C—H bond. The absorption peak of 1010–1105 cm^{-1} was caused by the Tensile vibration of C—OH, C—O—C and C—C, which indicated the existence of pyran ring structure (Kazemi, Khodaiyan, Labbafi, Hosseini, & Hojjati, 2019). The absorption peak at 886 cm^{-1} represented the glucose configuration is β-type (Shen, Jiang, Li, Zheng, & Zhu, 2017). The absorption peak at 833 cm^{-1} represented the ring vibration of the α-type glycosidic between GalA units (Szymanska-Chargot et al., 2015). The relative intensity of the peak at 833 cm^{-1} was much higher than that of 886 cm^{-1} peak, indicating that the linkages of CPDP and CP were mainly α-glycosidic with a small amount of β-glycosidic bonds.
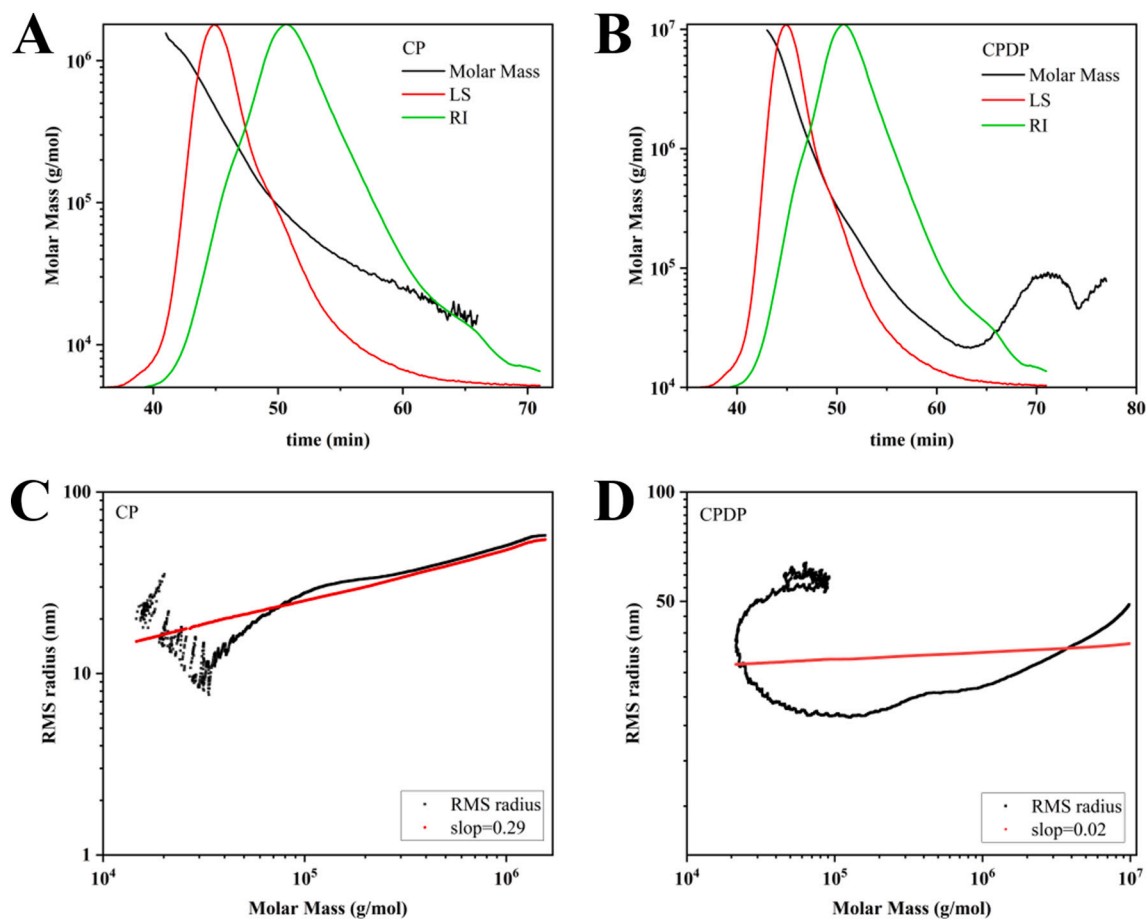
Fig. 2. Chromatograms of the molar mass distribution (A and B) and molecular configuration (C and D) of CP and CPDP.

Table 4
Molecular parameters of CP and CPDP.

	Molar mass (g/mol)		Polydispersity	RMS radius (nm)			Slop
	Mw	Mn	Mw/Mn	Rw	Rn	Rz	β
CP	1.326×10^5 (± 3.060 %) [b]	5.114×10^4 (± 0.350 %) [a]	2.592 (± 0.042 %) [b]	25.1 (± 0.1 %) [b]	17.9 (± 0.1 %) [b]	36.9 (± 0.1 %) [a]	0.29 (± 0.01 %) [a]
CPDP	2.006×10^5 (± 4.680 %) [a]	4.342×10^4 (± 0.140 %) [b]	4.621 (± 0.123 %) [a]	32.7 (± 0.3 %) [a]	34.6 (± 0.4 %) [a]	35.1 (± 0.1 %) [b]	0.02 (± 0.00 %) [b]

Mw: weight-average of molar mass; Mn: number-average of molar mass; RMS radius: root mean square radius of gyration; Rw: weight-average mean square radius of gyration; Rn: number-average mean square radius of gyration; Rz: z-average mean square radius of gyration.

Data are presented as "mean $\pm$ standard deviation", n = 3. Different lowercase letters in the same column indicate a significant difference between the CPDP and CP (p < 0.05).
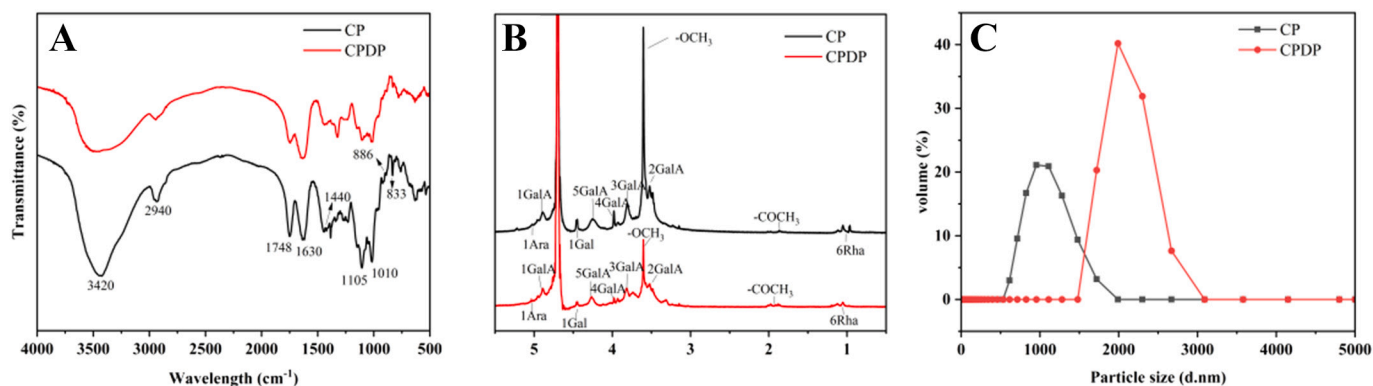

Fig. 3. FTIR spectrum (A), NMR spectrum (B) and particle size distribution (C) of CP and CPDP.

3.2.4. NMR spectroscopy analysis

The proton chemical shifts of pectin residues are shown in Table 5, which can correspond to the signal peaks of ^{1}H NMR in the Fig. 3B (Ovodova et al., 2009). GalA signals were observed in both CP and CPDP spectra, which confirmed the sample is a pectin (Zhang, Xie, Lan, Gong, & Wang, 2018). The signal peak around 3.60 ppm can be attributed to the methoxylatedified galacturonic acid unit (—OCH$_3$) proton, and the signal peak of CPDP was weaker than CP, indicating CPDP has lower DM, which is consistent with the FTIR spectroscopy results. The signal peak around 2.00 ppm was attributed to the acetyl (—COCH$_3$) proton (Khatib et al., 2017). The peaks around 1.05 ppm and 1.11 ppm corresponded to the O-2 and O-2,4 linked to H-6 of α-L-(1,2)-Rha (Kpodo et al., 2017). The signal peak at 5.07 ppm corresponded to H-1 of α-L-Ara and the signal peak at 4.47 ppm corresponded to H-1 of β-D-Gal. The monosaccharide composition results showed that the neutral sugar content of Gal, Rha and Ara were high in CPDP and CP, especially Gal, which were all confirmed in the NMR spectra.

3.3. Particle size and zeta potential analysis

The stability of the hydrocolloid system is determined by the electrostatic repulsion, which can be expressed by the zeta potential value (Munoz-Almagro et al., 2021). As shown in Table 2, both pectins were negatively charged at any pH values due to the presence of carboxyl groups on the pectin surface (Pan et al., 2022). The free carboxyl group on pectin molecule dissociates (releasing H^{+}) with the increase of pH value, resulting in higher absolute values of the negative zeta potential. For CP, the absolute value of the negative zeta potential increased significantly as the pH increased from 3 to 5, with little change in the pH range of 5–7. For CPDP, the absolute value of the negative zeta potential increased as the pH increased from 3 to 6, and then remained stable in the pH range of 6–7. The absolute values of the negative zeta potential of CPDP were smaller than those of CP in the pH range of 4–6, which is similar to the study of Zhang et al. (2021) that the absolute value of zeta potential of pectin rich in RG-I structure are smaller.
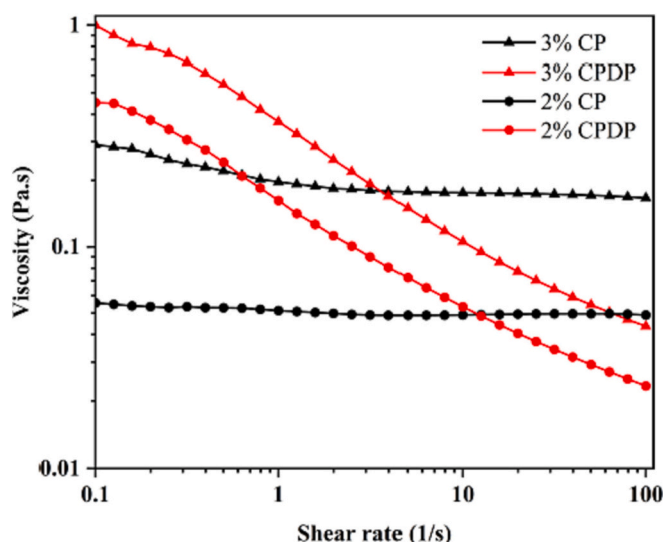
The particle size of pectin is a key factor affecting the viscosity, and pectin with larger particle size has greater viscosity (Wan, Chen, Huang, Liu, & Pan, 2019). PDI can be used to describe the particle size distribution of pectin. Pectin with larger PDI has wider particle size distribution. As shown in Fig. 3C, the volume peak of CP was between 531 and 1990 nm, while the volume peak of CPDP was between 1480 and 3090 nm. The particle size (2099 nm) and PDI (0.32) of CPDP were larger than the particle size (1243 nm) and PDI (0.20) of CP, which is consistent with the results of molecular weight testing.

3.4. Rheological properties analysis

The flow curves of CPDP and CP solutions under steady shear conditions are shown in Fig. 4. The apparent viscosity of CPDP and CP decreased with increasing shear rate, indicating the pseudoplastic fluid characteristics possibly due to the gradual weakening of the intermolecular strength of pectin (Chen et al., 2022). The shear-thinning mobility is mainly due to the increase in shear rate and the decrease in molecular chain entanglement (Cai, Qiu, Ding, Wu, & Yan, 2019; Wu, Cui, Eskin, & Goff, 2009). The molecules are easily reoriented with the flow direction, resulting in a significant decrease in apparent viscosity


Fig. 4. The shear-rate dependence of apparent viscosity of CP and CPDP solutions.

(Zhou, Bi, Chen, Wang, & Richel, 2021). The apparent viscosity of both CPDP and CP increased with increasing concentration. The apparent viscosity of CPDP was higher than that of CP at a shear rate of 0.1, which may be related to the arabinose enrichment of CPDP (Zheng et al., 2020). As the shear rate increased, CPDP exhibited significant shear thinning properties, while CP exhibited greater resistance to shear, which is may be due to the lower DM value and smaller hydrophobic interaction of CPDP, resulting in less decrease in apparent viscosity (Gan, Hj, Manaf, & Latiff, 2010).

3.5. Gel properties analysis

3.5.1. Morphology of pectin gels

As shown in Fig. 5A, when the pectin concentration was 5 g/L, neither CPDP nor CP could form a gel. When the pectin concentration increased to 10 g/L, CPDP could form stable gel, but the gel formed by CP could not be shaped and could not hang in the inverted vials. When the pectin concentration was increased to 15–25 g/L, both CPDP and CP
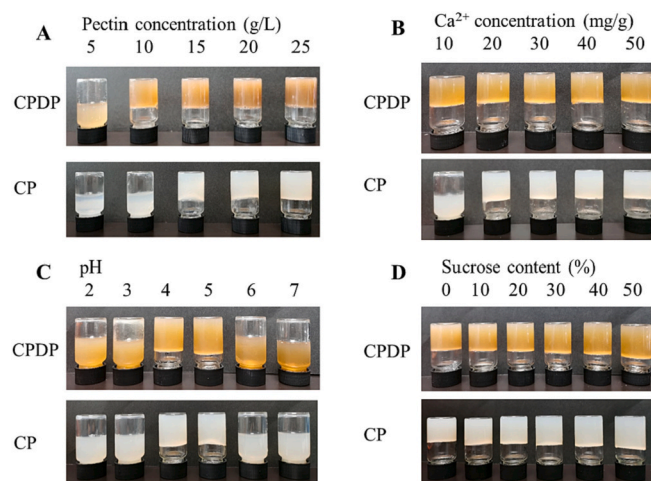
Fig. 5. Morphology of pectin gel formed at different pectin concentrations (A: Ca^{2+} concentration 30 mg/g, pH 4, sucrose content 30 %), Ca^{2+} concentration (B: pectin concentration 20 g/L, pH 4, sucrose content 30 %), pH value (C: pectin concentration 20 g/L, Ca^{2+} concentration 30 mg/g, sucrose content 30 %) and sucrose concentration (D: pectin concentration 20 g/L, Ca^{2+} concentration 30 mg/g, pH 4).

Table 5
^{1}H NMR chemical shifts of pectin.

Residue	Chemical shifts [1]H (ppm)					
	H-1	H-2	H-3	H-4	H-5	H-6
α-D-(1,4)-GalA	4.89	3.52	3.81	3.98	4.25	
α-L-Ara	5.07	4.12	3.95	4.13	3.82	
β-D-Gal	4.47	3.66	3.66	4.13	3.67	3.78
α-L-(1,2)-Rha	5.01	4.10	3.89	3.85	3.60	1.11

could form stable gels. As shown in Fig. 5B, the addition of 10 mg/g Ca^{2+} to CP could not form stable gels, but 10 mg/g Ca^{2+} to CPDP could form stable gels, indicating that the Ca^{2+} concentration required for CPDP to form a gel was lower than that of CP, which can save economic costs in industrial production by reducing the amount of Ca^{2+} ions added. Both pectins could form stable gels when the Ca^{2+} concentration was 20–50 mg/g. As shown in Fig. 5C, both pectins were unable to form gel network structures at pH = 2. When pH = 3, both pectins could form gels, but the formed gels were unstable and could not be hung in the inverted vial. When the pH value of pectin solution was 4–5, both pectins could form stable gel network structure. When the pH value further increased to 6–7, both pectins could not form gel network structures. Fig. 5D shows that sucrose had no significant effect on the formation of pectin gel network structure, and the two pectins could form stable gel even in the absence of sucrose.

It can be seen from the Fig. 5 that the transparency of CPDP gel was higher than that of CP gel, which may be due to the lower methoxy-esterification degree of CPDP (with more carboxyl groups containing hydrophilic -OH), thus forming smaller association zones (as shown in Fig. 8A-C, CPDP gels have smaller pores and more regular and ordered network structure) which made the CPDP gels more transparent. However, CP has a higher degree of methoxy-esterification (with more hydrophobic ester groups $-OCH_3$), so the larger association zones were formed (as shown in Fig. 8D-F, the gel network structure formed by CP has large and more disordered pores), resulting the CP gels more opaque (Liu et al., 2022). Therefore, CPDP gels are suitable for making soft candy, wound dressings and food-grade packaging materials, and CP gels are suitable for making solidified yogurt, jam and fat replacer (Ishwarya & Nisha, 2022).

3.5.2. Gel strength analysis

As shown in Fig. 6, the gel strength of CPDP was consistently higher than that of CP under any of the same conditions due to the lower esterification and longer neutral sugar side chains of CPDP. As the DM decreases, the sample has more free carboxyl groups that can interact with Ca^{2+} more efficiently, thus improving the gel rate (Gilsenan, Richardson, & Morris, 2000). Some studies found that the neutral sugar side chains in the RG-I region can stabilize the gel network structure (Makshakova, Faizullin, Mikshina, Gorshkova, & Zuev, 2018; Mikshina, Polina, Zuev, Yuriy, & Idiyatullin, 2017).

The concentration of pectin solution has a significant influence on the gel strength of pectin. As shown in Fig. 6A, the gel strength of pectin increased with the increase of the concentration of pectin solution. When the pectin concentration was 5 g/L, the gel strength of both CPDP and CP was 0. This is because there were fewer molecules in the solution when the pectin solution concentration was low, and the hydrogen bonding force and hydrophobic interaction force between pectin molecules were small, which were not enough to support the formation of a stable gel network structure of pectin. As the concentration of pectin increased, the space of pectin molecules decreased, the hydrophilic group hydroxyl (-OH) between molecules was more likely to form binding regions with hydrogen bonds, and more hydrophobic
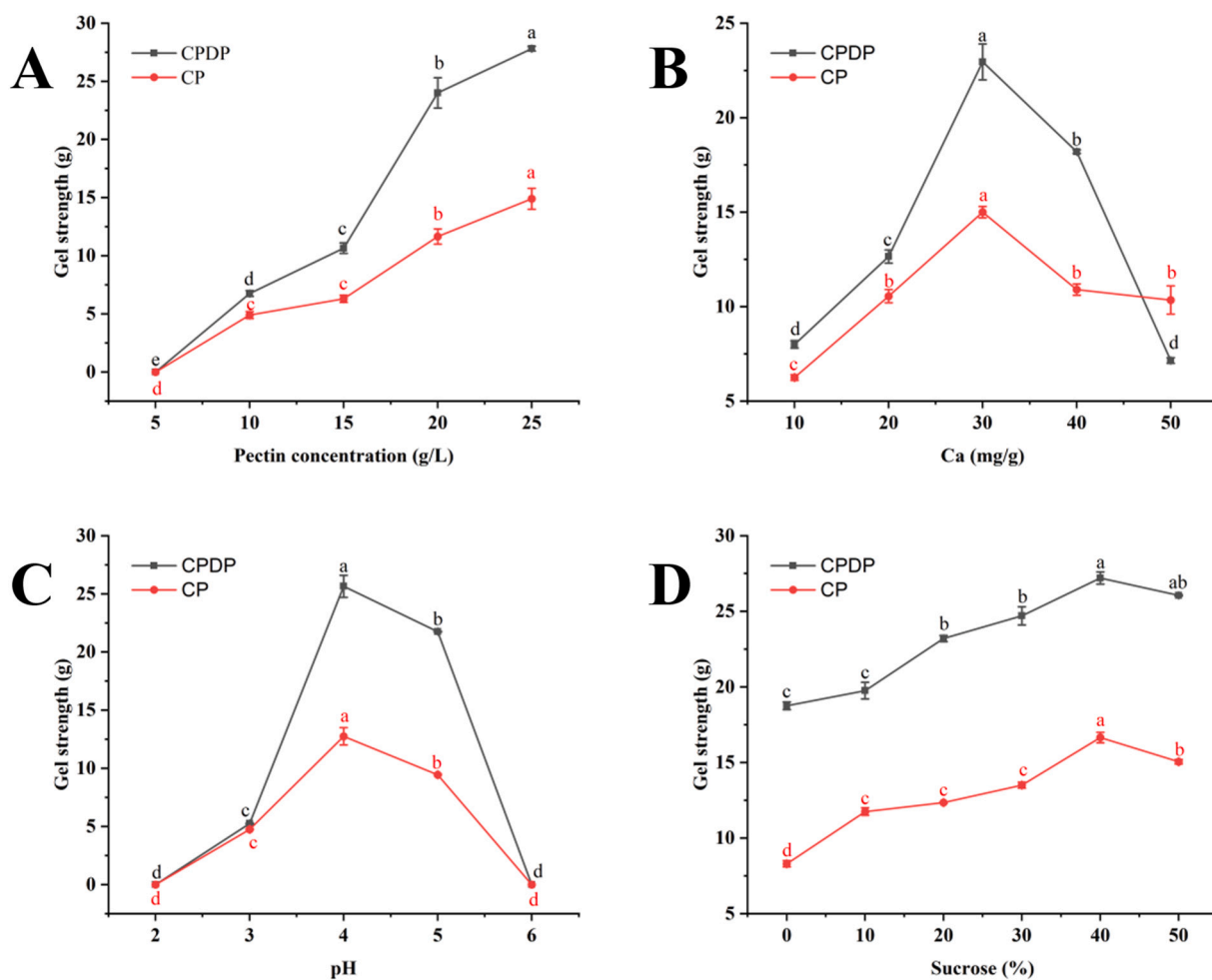

Fig. 6. Effects of pectin concentrations (A: Ca^{2+} concentration 30 mg/g, pH 4, sucrose content 30 %), Ca^{2+} concentration (B: pectin concentration 20 g/L, pH 4, sucrose content 30 %), pH value (C: pectin concentration 20 g/L, Ca^{2+} concentration 30 mg/g, sucrose content 30 %) and sucrose concentration (D: pectin concentration 20 g/L, Ca^{2+} concentration 30 mg/g, pH 4) on gel strength of CP and CPDP.

interactions were formed between methoxy ester groups (-OCH$_3$), thus improving the gel strength of pectin (Han et al., 2017). The gel strength of CPDP was higher than that of CP at any same pectin concentration due to the higher percentage of arabinose side chains in CPDP. Previous study found that arabinose side chains can enhance gel strength by enhancing chain entanglement to limit the movement of pectin chains (Zheng et al., 2020).

As shown in Fig. 6B, the gel strength of both pectins increased first and then decreased with the increase of Ca^{2+} concentration. The gel strength gradually increased when the concentration of Ca^{2+} in the pectin solution increased from 10 mg/L to 30 mg/L, because the higher concentration of Ca^{2+} in the solution, the more "egg-box" models formed by Ca^{2+} and COO$^-$ on the pectin molecule, the greater the gel strength. When the concentration of Ca^{2+} in the solution reached 30 mg/L, the gel strength reached the maximum. The gel strength of pectin decreased when the concentration of Ca^{2+} in the solution further increased to 50 mg/L. This is because the excess Ca^{2+} causes the precipitation to be larger than the gel, resulting in a phenomenon similar to pre-gelation, which leads to a large amount of water flowing out of the tissue, shrinking the network structure and reducing the gel strength. The gel strength of CPDP was lower than that of CP when the concentration of Ca^{2+} was 50 mg/L, indicating that the gel network formed by CPDP was more prone to dehydration and contraction at high Ca^{2+} concentration.

As shown in Fig. 6C, the gel strength of pectin first increased and then decreased with the increase of pH. When the pH value of pectin solution was 4.0, the gel strength of pectin reached the maximum, and the gel strengths of CP and CPDP were 12.75 g and 25.65 g, respectively. When the pH value of pectin solution was small, the carboxyl group in pectin solution was protonated (acquired H$^+$), then hydrogen bonding occurred between the undissociated carboxyl groups, and hydrophobic interaction occurred between methoxy ester groups. However, since the carboxyl groups existed mainly in the uncharged form (—COOH), they could not form a stable "egg-box" model with calcium ions and therefore the formed gel network structure was unstable. With the increase of pH, hydrogen bonding and hydrophobic interactions still exist. However, the gradual decrease of uncharged —COOH and the gradual increase of negatively charged COO$^-$ lead to an increase in the affinity of pectin with Ca^{2+} to form a stable "egg-box" model, which results in more ionic bonds (with electrostatic gravitational force) making the gel strength of the pectin solution gradually increase (Capel, Nicolai, Durand, Boulenguer, & Langendorff, 2006). The available ionic bonds reached their limit when the pH increased to 5. When the pH value was further increased to 7, the hydrogen bonds between the undissociated carboxyl groups gradually disappeared and hydrophobic interactions became very weak. Oversaturation of negatively charged COO$^-$ led to electrostatic repulsion between pectin chains thus prolonging the distance between pectin molecules and weakening the gel network structure.

As shown in Fig. 6D, sucrose concentration had the least effect on pectin gel strength relative to pectin concentration, pH value and Ca^{2+} concentration. The gel strength of CP ranged from 8.3 g - 16.65 g and that of CPDP ranged from 18.75 g - 26.05 g in the range of sucrose concentration of 0–50 %. The gel strength of both pectins increased and then decreased with increasing sucrose concentration in the solution. The gel strength tended to increase at 0–40 % sucrose concentration in the pectin solution because sucrose can provide more hydroxyl groups to stabilize the structure of the attachment zone during Ca^{2+}-induced gelation of low-methoxy pectin and promote hydrogen bonding to immobilize free water (Lofgren, Guillotin, & Hermansson, 2006). The gel strength tended to decrease when the sucrose concentration in the pectin solution was >40 %, which is due to the fact that too many sucrose molecules in the solution bind to water molecules, making the water in the pectin solution unable to form hydrogen bonds with the pectin molecules, thus decreasing the gel strength (Wang, Hua, Yang, Kang, & Zhang, 2014). Previous study stated that the addition of the right amount of sucrose to the low ester pectin solution not only helps to

increase the gel strength but also could improve the shape and color of the gels (Han et al., 2017).

3.5.3. Dynamic rheological analysis of pectin gels

The rheological characteristics and thermal stability of Ca^{2+}-induced pectin gels were further investigated. The storage modulus G′ (elastic modulus) reflects the ability of the gel to resist deformation, and the loss modulus G′′ (viscous modulus) represents the viscous characteristics of the gel (Maalej et al., 2016). The damping factor (tanδ) is the ratio of G′′ to G′, which represents the viscoelasticity of the pectin. The cross-over of G′ and G′′ (tanδ = G′′/G′ = 1) is defined as gel point (Holst, Kjoniksen, Bu, Sande, & Nystrom, 2006). Fig. 7A, B, C and D show the variation of storage modulus (G′) and loss modulus (G′′) with temperature during gel formation for CP and CPDP. It can be seen that the G′ of the gel increased with the decrease of temperature, which indicates the decrease in temperature promotes the gelation of CP and CPDP, making their gels more elastic at low temperatures. The G′ of CPDP gel was always higher than that of CP gel during cooling under the same temperature, indicating that the gel strength formed by CPDP is higher, which may be due to the lower DM and higher molecular weight of CPDP. The study of Yuliarti and Othman (2018) showed that the gel strength of pectin (characterized by G′) increased with decreasing pectin DM. The study of Gunter & Popeyko, 2016 showed that pectins with higher molecular weights have longer molecular chains and thus more Ca^{2+} binding sites, which contribute to the formation of network structures and improve the rheological properties of the gels (greater elastic modulus G′). Previous study showed that when the molecular weight of pectin is too low ($\leq$10 kDa), pectin is unable to form calcium gels due to the limited number of Ca^{2+} binding sites (Kyomugasho et al., 2018). In a word, CPDP has higher G′ than CP due to the lower DM and higher molecular weight.

The heating process of the gels were evaluated to investigate the thermal reversibility of pectin gels. During the heating process, the G′ of both pectins decreased and then increased. At the initial stage of heating from 5 to 65 °C, the G′ of both pectins decreased significantly, indicating that melting of the pectin gels occurred. At the later stage of heating from 65 to 95 °C, both pectins exhibited an increase in G′, which may be due to the loosening of the gel network structure during heating leading to Ca^{2+} redistribution in the gel network. A large amount of Ca^{2+} was dispersed in the loosened gel network and formed new ordered linkage regions involving stronger ionic bridges, thus leading to an increase in gel strength (Yuliarti & Othman, 2018). The changes of G′ and G′′ during the cooling process were not exactly consistent with the heating phase, indicating a hysteresis in the gel network structure during the cooling-heating process.

The frequency sweep of modulus G′ and G′′ are shown in Fig. 7E and F. When the oscillation frequency increased from 0.1 Hz to 10 Hz, the G′ of both pectin gels slightly increased, which might be due to the redistribution of Ca^{2+} and the formation of new ordered connection zones caused by the oscillation, thus increasing the gel elasticity. The G′ values were higher than G′′ values at all frequencies, which indicated both pectin gels showed elastic behavior.

3.5.4. FE-SEM analysis of pectin gels

The SEM images of CP and CPDP gels are shown in Fig. 8. The two pectin gel graphs showed network structures. The gel surface of CPDP was smooth and continuous, showing a more regular and orderly spatial network structure with smaller and more complete pores and thicker walls. This means that the gel network structure of CPDP was more stable with better deformation resistance (Wan et al., 2019), which is consistent with the gel strength. CP presented a more open and loose network structure. Previous studies reported that the number of consecutive non-methyl esterified galacturonic acid residues sufficient to form an "egg-box" model decreased as DM increased, and the reduced sensitivity of pectin to cation concentration led to weaker cross-linking, resulting in a weaker and more open gel structure (Fraeye et al., 2009).
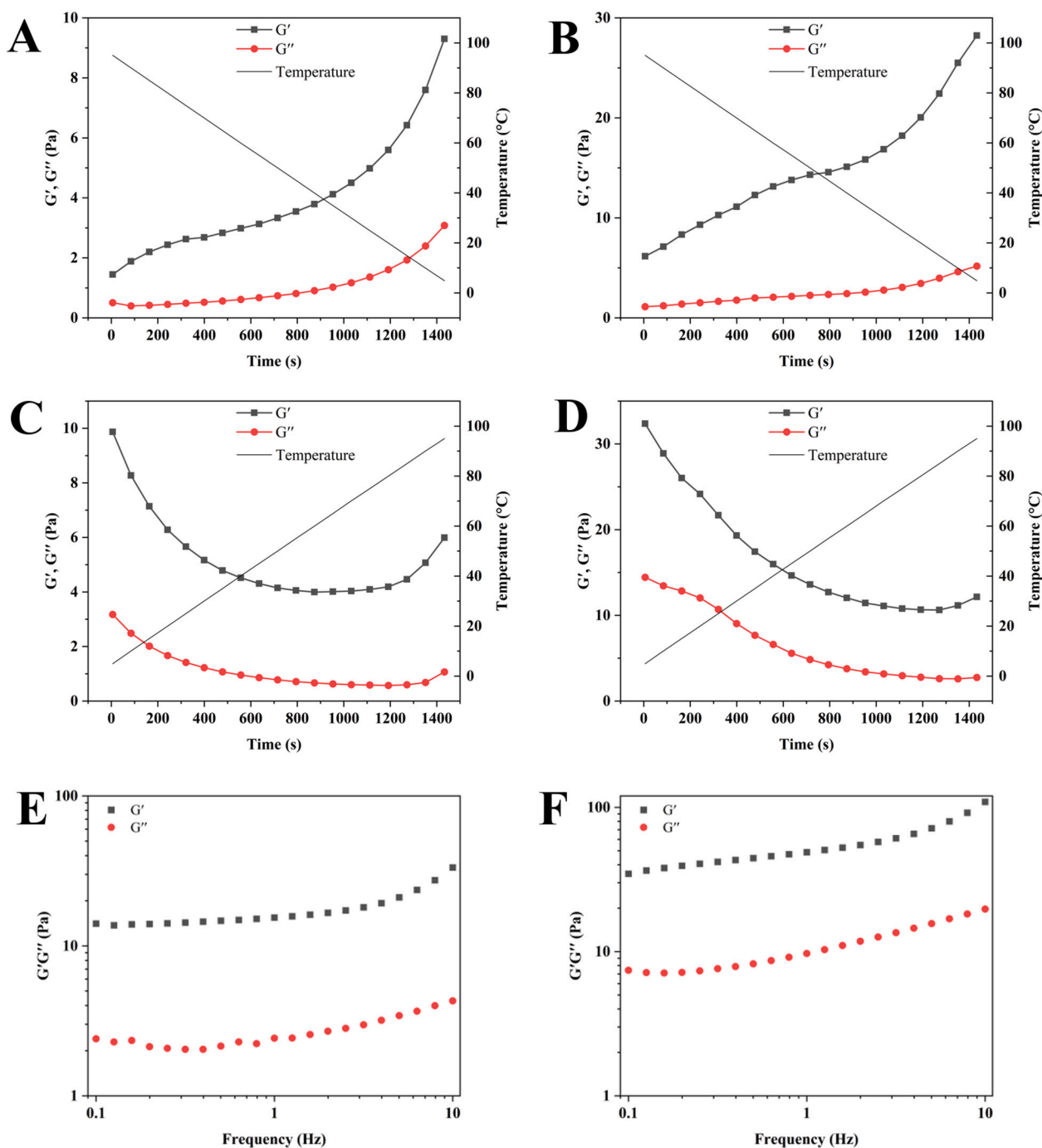
Fig. 7. Temperature dependence of storage modulus (G′) and loss modulus (G″) of gels during cooling processing (A: CP, B: CPDP) and heating processing (C: CP, D: CPDP), and frequency dependence of storage modulus (G′), loss modulus(G″) and damping factor (tanδ, G″/G′) of CP gel (E) and CPDP gel (F).

4. Conclusion

In this study, pectin was extracted from citrus physiological premature fruit drop by acid hydrolysis method. The monosaccharide composition test results showed that CPDP had abundant RG-I region and long side chains of Ara and Gal, which corresponded to a larger molecular weight and apparent viscosity. CPDP was LMP, which indicated that citrus physiological premature fruit drop could be used as a new natural source for extracting low-methoxylated pectin. LMP can form gel without sugar. The textural, rheological and SEM results showed that the gel formed by CPDP had higher gel strength, storage modulus and stable network structure, which indicates that CPDP has great potential for application in the low-sugar food industry, such as low-sugar jams, jellies and other foods.

CRediT authorship contribution statement

Tingting Qi: Methodology, Software, Data Curation, Formal analysis, Investigation, Writing - Original Draft.
Jingnan Ren: Conceptualization, Methodology, Software, Project administration.
Xiao Li: Writing- Reviewing and Editing.
Qi An: Validation.
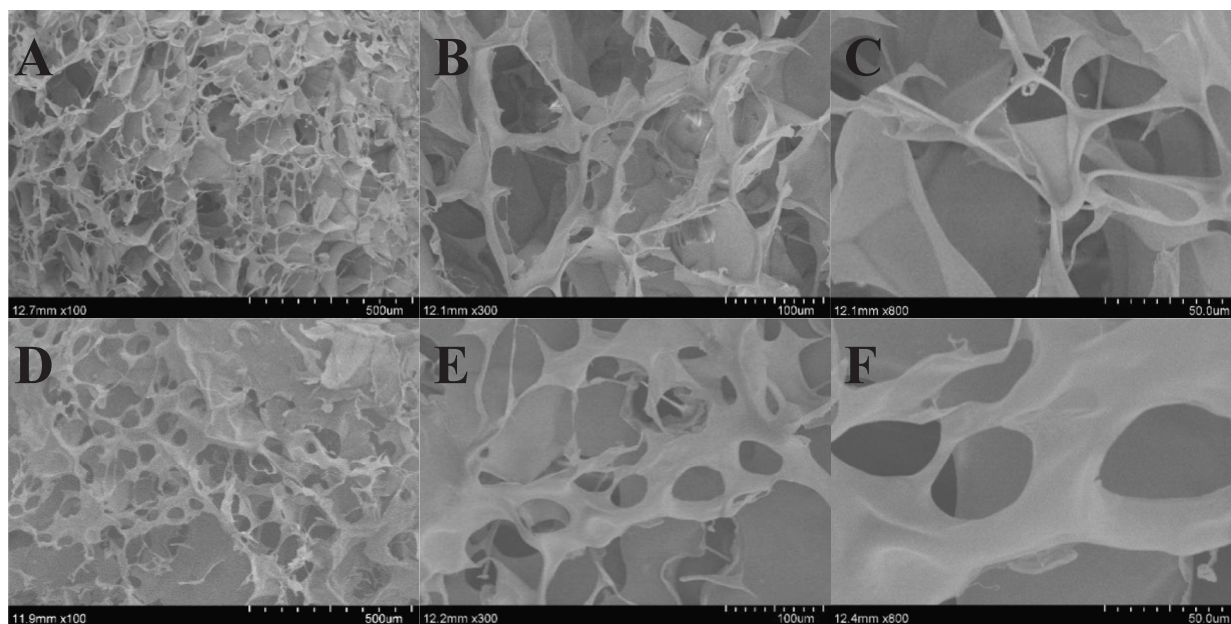**Nawei Zhang**: Software.

Fig. 8. Microstructure of CP gel (A: 100×, B: 300×, C: 800×) and CPDP gel (D: 100×, E: 300×, F: 800×).

Xiao Jia: Data Curation.
Siyi Pan: Supervision.
Gang Fan: Conceptualization, Resources, Writing- Reviewing and Editing, Funding acquisition.
Zhifeng Zhang:Funding
Kangning Wu:Software

Declaration of competing interest

We declare that there are no known competing financial interests or personal relationships that could have appeared to influence the work reported in this paper

We declare that this manuscript or part of its content is not submitted elsewhere, nor is it under consideration for submission elsewhere.

Data availability

Data will be made available on request.

Acknowledgments

Appendix A. Supplementary data

Supplementary data to this article can be found online at https://doi.org/10.1016/j.carbpol.2023.120682.

References

Cai, W. D., Hu, T., & Huang, Q. L. (2021). A polysaccharide from Lignosus rhinocerotis sclerotia: Self-healing properties and the effect of temperature on its rheological behavior. *Carbohydrate Polymers, 267*.

Cai, W.-D., Qiu, W.-Y., Ding, Z.-C., Wu, L.-X., & Yan, J.-K. (2019). Conformational and rheological properties of a quaternary ammonium salt of curdlan. *Food Chemistry, 280*, 130–138.

Capel, F., Nicolai, T., Durand, D., Boulenguer, P., & Langendorff, V. (2006). Calcium and acid induced gelation of (amidated) low methoxyl pectin. *Food Hydrocolloids, 20*(6), 901–907.

Chandel, V., Biswas, D., Roy, S., Vaidya, D., Verma, A., & Gupta, A. (2022). Current advancements in pectin: Extraction, properties and multifunctional applications. *Foods, 11*(17).

Chen, J., Cheng, H., Wu, D., Linhardt, R. J., Zhi, Z., Yan, L., & Ye, X. (2016). Green recovery of pectic polysaccharides from citrus canning processing water. *Journal of Cleaner Production, 144*(FEB.15), 459–469.

Chen, S., Xiao, L., Li, S., Meng, T., Wang, L., & Zhang, W. (2022). The effect of sonication-synergistic natural deep eutectic solvents on extraction yield, structural and physicochemical properties of pectins extracted from mango peels. *Ultrasonics Sonochemistry, 86*, Article 106045.

Cheng, Y., Wang, W., Zhang, R., Zhai, X., & Hou, H. (2021). Effect of gelatin bloom values on the physicochemical properties of starch/gelatin-beeswax composite films fabricated by extrusion blowing. *Food Hydrocolloids, 113*.

Cho, E.-H., Jung, H.-T., Lee, B.-H., Kim, H.-S., Rhee, J.-K., & Yoo, S.-H. (2019). Green process development for apple-peel pectin production by organic acid extraction. *Carbohydrate Polymers, 204*, 97–103.

Colodel, C., Vriesmann, L. C., & Lucia, D. (2019). Rheological characterization of a pectin extracted from ponkan (Citrus reticulata blanco cv. ponkan) peel. *Food Hydrocolloids, 94*(SEP.), 326–332.

Cui, J., Zhao, C., Zhao, S., Tian, G., Wang, F., Li, C., & Zheng, J. (2020). Alkali plus cellulase-extracted citrus pectins exhibit compact conformation and good fermentation properties. *Food Hydrocolloids, 108*, Article 106079.

Dasilva, J. A. L., Goncalves, M. P., & Rao, M. A. (1995). Kinetics and thermal behaviour of the structure formation process in HMP/sucrose gelation. *International Journal of Biological Macromolecules, 17*(1), 25–32.

Deng, Z., Pan, Y., Chen, W., Chen, W., Yun, Y., Zhong, Q., & Chen, H. (2020). Effects of cultivar and growth region on the structural, emulsifying and rheological characteristic of mango peel pectin. *Food Hydrocolloids, 103*.

Ferreira, D. C. M., Ferreira, S. O., de Alvarenga, E. S., Soares, N. D. F. F., Coimbra, J. S. D. R., & de Oliveira, E. B. (2022). Polyelectrolyte complexes (PECs) obtained from chitosan and carboxymethylcellulose: A physicochemical and microstructural study. *Carbohydrate Polymer Technologies and Applications, 3*.

Fraeye, I., Duvetter, T., Doungla, E., Van Loey, A., & Hendrickx, M. (2010). Fine-tuning the properties of pectin calcium gels by control of pectin fine structure, gel composition and environmental conditions. *Trends in Food Science & Technology, 21* (5), 219–228.

Fraeye, U., Doungla, E., Duvetter, T., Moldenaers, P., Loey, A. V., & Hendrickx, M. (2009). Influence of intrinsic and extrinsic factors on rheology of pectin-calcium gels. *Food Hydrocolloids, 23*(8), 2069–2077.

Galván, Z. R. N., Soares, L. D. S., Medeiros, E. A. A., Soares, N. D. F. F., Ramos, A. M., Coimbra, J. S. D. R., & de Oliveira, E. B. (2018). Rheological properties of aqueous dispersions of xanthan gum containing different chloride salts are impacted by both sizes and net electric charges of the cations. *Food Biophys., 13*(2), 186–197.

Gan, C. Y., Hj, N., Manaf, A., & Latiff, A. A. (2010). Physico-chemical properties of alcohol precipitate pectin-like polysaccharides from Parkia speciosa pod. *Food Hydrocolloids, 24*(5), 471–478.

Gilsenan, P. M., Richardson, R. K., & Morris, E. R. (2000). Thermally reversible acid-induced gelation of low-methoxy pectin. *Carbohydrate Polymers, 41*(4), 339–349.

Gunter, E. A., & Popeyko, O. V. (2016). Calcium pectinate gel beads obtained from callus cultures pectins as promising systems for colon-targeted drug delivery. *Carbohydrate Polymers, 147*, 490–499.

Guo, X., Guo, X., Yu, S., & Kong, F. (2018). Influences of the different chemical components of sugar beet pectin on the emulsifying performance of conjugates

formed between sugar beet pectin and whey protein isolate. *Food Hydrocolloids, 82*, 1–10.

Han, W. Y., Meng, Y. H., Hu, C. Y., Dong, G. R., Qu, Y. L., Deng, H., & Guo, Y. R. (2017). Mathematical model of Ca2+ concentration, pH, pectin concentration and soluble solids (sucrose) on the gelation of low methoxyl pectin. *Food Hydrocolloids, 66*, 37–48.

Holst, P. S., Kjoniksen, A. L., Bu, H. T., Sande, S. A., & Nystrom, B. (2006). Rheological properties of pH-induced association and gelation of pectin. *Polymer Bulletin, 56* (2–3), 239–246.

Hosseini, S. S., Khodaiyan, F., Kazemi, M., & Najari, Z. (2019). Optimization and characterization of pectin extracted from sour orange peel by ultrasound assisted method. *International Journal of Biological Macromolecules, 125*, 621–629.

Huang, S., Tu, Z., Sha, X., Wang, H., Hu, Y., & Hu, Z. (2020). Gelling properties and interaction analysis of fish gelatin–low-methoxyl pectin system with different concentrations of Ca2+. *LWT - Food Science and Technology, 132*.

Ishwarya, S. P. R. S., & Nisha, P. (2022). Advances and prospects in the food applications of pectin hydrogels. *Critical Reviews in Food Science and Nutrition, 62*(16), 4393–4417.

Jafari, F., Khodaiyan, F., Kiani, H., & Hosseini, S. S. (2017). Pectin from carrot pomace: Optimization of extraction and physicochemical properties. *Carbohydrate Polymers, 157*, 1315–1322.

Kang, J., Hua, X., Yang, R., Chen, Y., & Yang, H. (2015). Characterization of natural low-methoxyl pectin from sunflower head extracted by sodium citrate and purified by ultrafiltration. *Food Chemistry, 180*, 98–105.

Kazemi, M., Khodaiyan, F., Labbafi, M., Hosseini, S. S., & Hojjati, M. (2019). Pistachio green hull pectin: Optimization of microwave-assisted extraction and evaluation of its physicochemical, structural and functional properties. *Food Chemistry, 271*, 663–672.

Khatib, M., Giuliani, C., Rossi, F., Adessi, A., Al-Tamimi, A., Mazzola, G., & Mulinacci, N. (2017). Polysaccharides from by-products of the wonderful and laffan pomegranate varieties: New insight into extraction and characterization. *Food Chemistry, 235*, 58–66.

Kpodo, F. M., Agbenorhevi, J. K., Alba, K., Bingham, R. J., Oduro, I. N., Morris, G. A., & Kontogiorgos, V. (2017). Pectin isolation and characterization from six okra genotypes. *Food Hydrocolloids, 72*, 323–330.

Kyomugasho, C., Munyensanga, C., Celus, M., Van de Walle, D., Dewettinck, K., Van Loey, A. M., & Hendrickx, M. E. (2018). Molar mass influence on pectin-Ca2+ adsorption capacity, interaction energy and associated functionality: Gel microstructure and stiffness. *Food Hydrocolloids, 85*, 331–342.

Li, Q., Li, J., Li, H., Xu, R., Yuan, Y., & Cao, J. (2019). Physicochemical properties and functional bioactivies of different bonding state polysaccharides extracted from tomato fruit. *Carbohydrate Polymers, 219*, 181–190.

Liu, J., Cui, L., Shi, Y., Zhang, Q., Zhuang, Y., & Fei, P. (2022). Preparation of hydrophobic composite membranes based on carboxymethyl cellulose and modified pectin: Effects of grafting a long-chain saturated fatty acid. *International Journal of Biological Macromolecules, 222*, 2318–2326.

Lofgren, C., Guillotin, S., & Hermansson, A. M. (2006). Microstructure and kinetic rheological behavior of amidated and nonamidated LM pectin gels. *Biomacromolecules, 7*(1), 114–121.

Maalej, H., Hmidet, N., Boisset, C., Bayma, E., Heyraud, A., & Nasri, M. (2016). Rheological and emulsifying properties of a gel-like exopolysaccharide produced by pseudomonas stutzeri AS22. *Food Hydrocolloids, 52*, 634–647.

Makshakova, O. N., Faizullin, D. A., Mikshina, P. V., Gorshkova, T. A., & Zuev, Y. F. (2018). Spatial structures of rhamnogalacturonan I in gel and colloidal solution identified by 1D and 2D-FTIR spectroscopy. *Carbohydrate Polymers, 192*, 231–239.

Makshakova, O. N., Safarova, E. R., & Zuev, Y. F. (2021). Structural insights in interactions between RNase from bacillus intermedius and rhamnogalacturonan I from potato. *Carbohydrate Polymers, 251*.

Mikshina, Polina, V., Zuev, Yuriy, F., & Idiyatullin. (2017). Gelation of rhamnogalacturonan I is based on galactan side chain interaction and does not involve chemical modifications. *Carbohydrate Polymers: Scientific and Technological Aspects of Industrially Important Polysaccharides, 171*, 143–151.

Munoz-Almagro, N., Vendrell-Calatayud, M., Mendez-Albinana, P., Moreno, R., Cano, M. P., & Villamiel, M. (2021). Extraction optimization and structural characterization of pectin from persimmon fruit (Diospyros kaki Thunb. var. Rojo brillante). *Carbohydrate Polymers, 272*.

Munoz-Almagro, N., Villamiel, M., Wilde, P. J., Gunning, A. P., & Montilla, A. (2021). Effect of sucrose substitution with stevia and saccharin on rheological properties of gels from sunflower pectins. *Food Hydrocolloids, 120*.

Nakauma, M., Funami, T., Noda, S., Ishihara, S., Al-Assaf, S., Nishinari, K., & Phillips, G. O. (2008). Comparison of sugar beet pectin, soybean soluble polysaccharide, and gum arabic as food emulsifiers. 1. Effect of concentration, pH, and salts on the emulsifying properties. *Food Hydrocolloids, 22*(7), 1254–1267.

Nguyen, H. H. D., Nguyen, H. V. H., & Savage, G. P. (2019). Properties of pectin extracted from Vietnamese mango peels. *Foods, 8*(12).

O'Neill, M., Albersheim, P., & Darvill, A. (1990). The pectic polysaccharides of primary cell walls. In D. M. Dey (Ed.), *2. Methods in Plant Biochemistry* (pp. 415–441).

Ovodova, R. G., Golovchenko, V. V., Popov, S. V., Popova, G. Y., Paderin, N. M., Shashkov, A. S., et al. (2009). Chemical composition and anti-inflammatory activity of pectic polysaccharide isolated from celery stalks. *Food Chemistry, 114*(2), 610e615.

Pan, X., Zhao, W. T., Wang, Y. X., Xu, Y. Y., Zhang, W. T., Lao, F., & Wu, J. H. (2022). Physicochemical and structural properties of three pectin fractions from muskmelon (Cucumis melo) and their correlation with juice cloud stability. *Food Hydrocolloids, 124*.

Qiu, C. Y., Huang, Y., Li, A. J., Ma, D., & Wang, Y. (2018). Fabrication and characterization of oleogel stabilized by gelatin-polyphenol-polysaccharides nanocomplexes. *Journal of Agricultural and Food Chemistry, 66*(50), 13243–13252.

Ren, J.-N., Hou, Y.-Y., Fan, G., Zhang, L.-L., Li, X., Yin, K., & Pan, S.-Y. (2019). Extraction of orange pectin based on the interaction between sodium caseinate and pectin. *Food Chemistry, 283*, 265–274.

Ridley, B. L., O'Neill, M. A., & Mohnen, D. A. (2001). Pectins: Structure, biosynthesis, and oligogalacturonide-related signaling. *Phytochemistry, 57*(6), 929–967.

Santos, E. E., Amaro, R. C., Cid Bustamante, C. C., Andrade Guerra, M. H., Soares, L. C., & Santos Froes, R. E. (2020). Extraction of pectin from agroindustrial residue with an ecofriendly solvent: Use of FTIR and chemometrics to differentiate pectins according to degree of methyl esterification. *Food Hydrocolloids, 107*, Article 105921.

Shen, C.-Y., Jiang, J.-G., Li, M.-Q., Zheng, C.-Y., & Zhu, W. (2017). Structural characterization and immunomodulatory activity of novel polysaccharides from Citrus aurantium Linn. Variant Amara engl. *Journal of Functional Foods, 35*, 352–362.

Soares, L. S., Perim, R. B., de Alvarenga, E. S., Guimaraes, L. M., Teixeira, A., Coimbra, J., & de Oliveira, E. B. (2019). Insights on physicochemical aspects of chitosan dispersion in aqueous solutions of acetic, glycolic, propionic or lactic acid. *International Journal of Biological Macromolecules, 128*, 140–148.

Su, D. L., Li, P. J., Quek, S. Y., Huang, Z. Q., Yuan, Y. J., Li, G. Y., & Shan, Y. (2019). Efficient extraction and characterization of pectin from orange peel by a combined surfactant and microwave assisted process. *Food Chemistry, 286*(JUL.15), 1–7.

Szymanska-Chargot, M., Chylinska, M., Kruk, B., & Zdunek, A. (2015). Combining FT-IR spectroscopy and multivariate analysis for qualitative and quantitative analysis of the cell wall composition changes during apples development. *Carbohydrate Polymers, 115*, 93–103.

Thakur, B. R., Singh, R. K., & Handa, A. K. (1997). Chemistry and uses of pectin - A review. *Critical Reviews in Food Science and Nutrition, 37*(1), 47–73.

Wan, L., Chen, Q., Huang, M., Liu, F., & Pan, S. (2019). Physiochemical, rheological and emulsifying properties of low methoxyl pectin prepared by high hydrostatic pressure-assisted enzymatic, conventional enzymatic, and alkaline de-esterification: A comparison study. *Food Hydrocolloids, 93*, 146–155.

Wan, L., Wang, H. Y., Zhu, Y., Pan, S. Y., Cai, R., Liu, F. X., & Pan, S. Y. (2019). Comparative study on gelling properties of low methoxyl pectin prepared by high hydrostatic pressure-assisted enzymatic, atmospheric enzymatic, and alkaline de-esterification. *Carbohydrate Polymers, 226*.

Wan, L., Yang, Z., Cai, R., Pan, S., Liu, F., & Pan, S. (2021). Calcium-induced-gel properties for low methoxyl pectin in the presence of different sugar alcohols. *Food Hydrocolloids, 112*.

Wang, K., Hua, X., Yang, R. J., Kang, J. Q., & Zhang, W. B. (2014). Hydrodynamic behavior and gelling properties of sunflower head pectin in the presence of sodium salts. *Food Hydrocolloids, 36*, 238–244.

Wang, W., Ma, X., Jiang, P., Hu, L., Zhi, Z., Chen, J., & Liu, D. (2016). Characterization of pectin from grapefruit peel: A comparison of ultrasound-assisted and conventional heating extractions. *Food Hydrocolloids, 61*, 730–739.

Wang, X., Chen, Q., & Lu, X. (2014). Pectin extracted from apple pomace and citrus peel by subcritical water. *Food Hydrocolloids, 38*, 129–137.

Wu, D. T., Meng, L. Z., Wang, L. Y., Lv, G. P., Cheong, K. L., Hu, D. J., & Li, S. P. (2014). Chain conformation and immunomodulatory activity of a hyperbranched polysaccharide from cordyceps sinensis. *Carbohydr Polymers, 110*, 405–414.

Wu, Y., Cui, W., Eskin, N. A. M., & Goff, H. D. (2009). An investigation of four commercial galactomannans on their emulsion and theological properties. *Food Research International, 42*(8), 1141–1146.

Wyatt, P. J. (1993). Light scattering and the absolute characterization of macromolecules. *Analytica Chimica Acta, 272*(1), 1–40.

Xu, S., Xu, Xu, Xu, & Zhang, L. (2012). Branching structure and chain conformation of water-soluble glucan extracted from Auricularia auricula-judae. *Journal of Agricultural and Food Chemistry, 60*(13), 3498–3506.

Yan, J.-K., Wang, C., Qiu, W.-Y., Chen, T.-T., Yang, Y., Wang, W.-H., & Zhang, H.-N. (2021). Ultrasonic treatment at different pH values affects the macromolecular, structural, and rheological characteristics of citrus pectin. *Food Chemistry, 341*.

Yuliarti, O., & Othman, R. M. B. (2018). Temperature dependence of acid and calcium-induced low-methoxyl pectin gel extracted from cyclea barbata miers. *Food Hydrocolloids, 81*, 300–311.

Zhao, W., Kim, Y., & Cameron, R. G. (2022). A novel multiplex lateral flow assay for rapid assessment of pectin structural/functional properties. *Food Hydrocolloids, 133*.

Zhang, L. M., Zheng, J. Q., Wang, Y., Ye, X. Q., Chen, S. G., Pan, H. B., & Chen, J. L. (2022). Fabrication of rhamnogalacturonan-I enriched pectin-based emulsion gels for protection and sustained release of curcumin. *Food Hydrocolloids, 128*.

Zhang, S., He, Z., Cheng, Y., Xu, F., Cheng, X., & Wu, P. (2021). Physicochemical characterization and emulsifying properties evaluation of RG-I enriched pectic polysaccharides from cerasus humilis. *Carbohydrate Polymers, 260*.

Zhang, S., Waterhouse, G. I. N., Xu, F., He, Z., Du, Y., Lian, Y., & Sun-Waterhouse, D. (2021). Recent advances in utilization of pectins in biomedical applications: A review focusing on molecular structure-directing health-promoting properties. *Critical Reviews in Food Science and Nutrition*, 1–34.

Zhang, W., Xie, F., Lan, X., Gong, S., & Wang, Z. (2018). Characteristics of pectin from black cherry tomato waste modified by dynamic high-pressure microfluidization. *Journal of Food Engineering, 216*, 90–97.

Zhao, B., Wang, C., Zeng, Z., & Xu, Y. (2021). Study on the extraction process of pectin from grapefruit peel based on steam explosion technology. *IOP Conference Series: Earth and Environmental Science, 792*(1), 012008 (012007pp).

Zhao, W., Chai, D.-D., Li, H.-M., Chen, T., & Tang, Y.-J. (2014). Significance of metal ion supplementation in the fermentation medium on the structure and anti-tumor

activity of tuber polysaccharides produced by submerged culture of tuber melanosporum. *Process Biochemistry, 49*(12), 2030–2038.

Zheng, J. Q., Chen, J. L., Zhang, H., Wu, D. M., Ye, X. Q., Linardt, R. J., & Chen, S. G. (2020). Gelling mechanism of RG-I enriched citrus pectin: Role of arabinose side-chains in cation- and acid-induced gelation. *Food Hydrocolloids, 101*.

Zhou, M., Bi, J., Chen, J., Wang, R., & Richel, A. (2021). Impact of pectin characteristics on lipid digestion under simulated gastrointestinal conditions: Comparison of water-soluble pectins extracted from different sources. *Food Hydrocolloids, 112*.